

# Revisit Human-Scene Interaction via Space Occupancy

Xinpeng Liu<sup>1\*</sup> Haowen Hou<sup>1,2\*†</sup> Yanchao Yang<sup>3</sup> Yong-Lu Li<sup>1‡</sup> Cewu Lu<sup>1</sup>  
<sup>1</sup>Shanghai Jiao Tong University <sup>2</sup>Soochow University <sup>3</sup>The University of Hong Kong

xinpengliu0907@gmail.com, haowenhoutoutlook.com, yanchaoy@hku.hk, {yonglu.li, lucewu}@sjtu.edu.cn

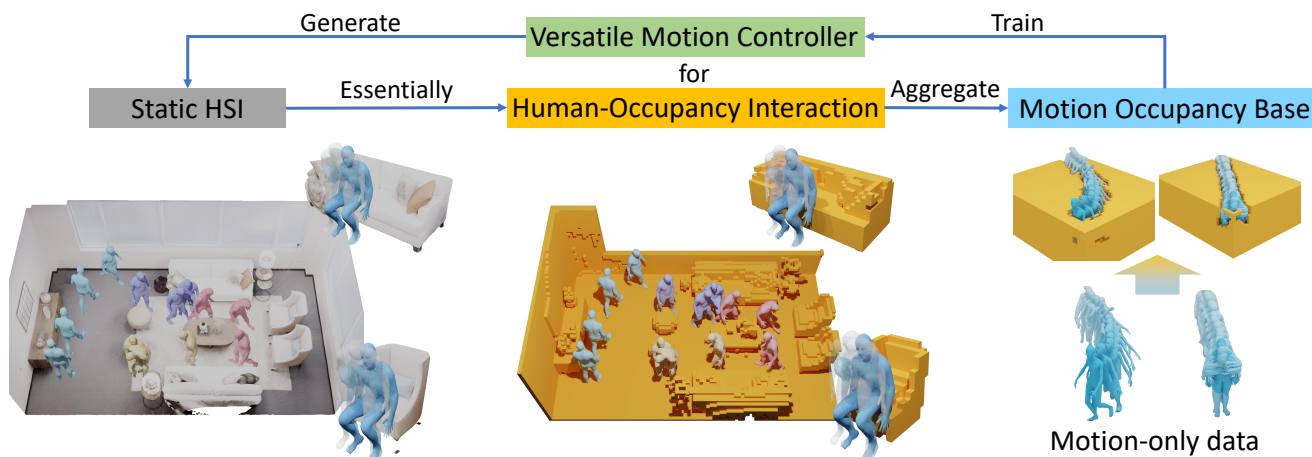


Figure 1. In this paper, we propose a new perspective that interacting with scenes is essentially interacting with its space occupancy for static HSI. In this view, we can unify motion-only data into a unified human-occupancy knowledge base and train a versatile Human-Occupancy Interaction controller upon it, achieving stable generation under various scenarios.

## Abstract

Human-scene Interaction (HSI) generation is a challenging task and crucial for various downstream tasks. However, one of the major obstacles is the limited data scale. High-quality data with simultaneously captured human and 3D environments is rare, resulting in limited data diversity and complexity. In this work, we argue that interaction with a scene is essentially interacting with the space occupancy of the scene from an abstract physical perspective, leading us to a unified novel view of Human-Occupancy Interaction. By treating pure motion sequences as records of humans interacting with invisible scene occupancy, we can aggregate motion-only data into a large-scale paired human-occupancy interaction database: Motion Occupancy Base (MOB). Thus, the need for costly paired motion-scene datasets with high-quality scene scans can be substantially alleviated. With this new unified view of Human-Occupancy interaction, a single motion controller

is proposed to reach the target state given the surrounding occupancy. Once trained on MOB with complex occupancy layout, the controller could handle cramped scenes and generalize well to general scenes with limited complexity. With no GT 3D scenes for training, our method can generate realistic and stable HSI motions in diverse scenarios, including both static and dynamic scenes. **Our code and data would be made publicly available at [this link](#).**

## 1. Introduction

Human-Scene Interaction (HSI) generation has been an active field recently with its wide application in animation [40] and embodied AI [38, 39, 42]. For ideal HSI generation, models should be able to control the flexible articulated human body to conduct various motions in highly complex 3D environments, considering geometry constraints, motion feasibility, and motion diversity. In this paper, we focus on interactions that would not change the scene, which we refer to as static HSI.

The **limited data scale** is a major obstacle for static HSI generation. High-quality data with simultaneously captured

\*The first two authors contributed equally.

†Work done during an internship at Shanghai Jiao Tong University.

‡Yong-Lu Li is the corresponding author.

human and 3D scenes is rare and expensive. Some efforts [17, 62] collected data only for a narrow range of target objects. Widely adopted PROX [16] contains only 60 clips with limited diversity and complexity. HUMANISE [51] synthesized paired data by fitting motion from large-scale motion base AMASS [30] into various scenes. CIRCLE [1] put the scenes in VR applications to reduce the cost. In light of these challenges, we pursue to dig into the essence of static HSI and revisit it from a space occupancy view.

Space occupancy is usually identified as an elementary constraint for HSI: humans and scenes cannot occupy the same space simultaneously, which prevents humans from penetrating scenes. We argue that occupancy is inherently the primary factor, especially for static HSI, which is essentially interaction with the scene occupancy. As shown in Fig. 1, sitting on a chair is practically sitting on a chair-shaped *solid being*. The chair’s occupancy allows us to rest our weight upon it, offering options to sit or stand. Its height and shape naturally invite sitting, which is a prime factor of interaction from a physical/affordance perspective. While elements like textures and labels (*e.g.*, identifying it as a “chair” semantically) influence our likelihood of choosing to sit, they are secondary to the chair’s physical form. The occupancy of scenes, therefore, offers a range of affordances and delineates potential interaction types, establishing an initial probability distribution for choices. This is primarily accessible to the model and should be learned well at first.

In view of this, *paired* motion-scene datasets become less necessary, inspiring us to revisit large-scale motion datasets. Instead of treating motion-only data as locomotion knowledge bases like existing efforts [63, 66], we transform them into a comprehensive Human-Occupancy Interaction database, which we call the Motion Occupancy Base (MOB). For any given motion sequence, we first identify the space occupied by the human at any time in the sequence. The remaining space, not occupied during the whole sequence, is conceptualized as the “scene”. In this framework, the motion becomes a record of interaction with these defined space occupancies. As a result, MOB aggregates enormous paired human-occupancy data from existing large-scale motion-only data. Compared to current datasets [1, 16, 51], MOB presents more *complex* and *stringent geometric constraints*, pushing the model to the limit in interacting with space occupancy.

How do we exploit the aggregated MOB for static HSI? Previous approaches generally provided two different answers. Some [1, 21, 51, 67] adopt an end-to-end pipeline from scene to motion, which is straightforward but inflexible without the ability to generate ultra-long motions and interact with dynamic scenes. Some [49, 50, 66] typically decouple HSI into interaction and locomotion, adopting a two-stage paradigm: first generating key interaction frames

and then synthesizing locomotion between them, with the help of methods like path-finding algorithms. However, this decomposition overlooks the integrated nature of locomotion and interaction, like simultaneous arm movement and walking to navigate obstacles. Our approach, rooted in space occupancy, reconceptualizes locomotion and interaction as a unified Human-Occupancy Interaction. We develop an auto-regressive Human-Occupancy Interaction controller for motion generation. The controller processes various inputs, including surrounding occupancy and target locations, as control signals at each time step, producing future motion predictions. Additionally, we introduce a field regulation module for enhanced collision avoidance. There are three major advantages of our controller. **First**, by learning from the challenging cases in MOB, it could handle complex scenes but also generalize well to regular simpler scenarios. **Second**, its versatility accommodates any static HSI without the need to switch between models for locomotion and interactions. **Third**, its auto-regressive nature allows it to adapt to dynamic environments such as an automatic door, a capability lacking in previous methods. Through extensive experiments, we show our controller performs effectively across various settings, even without training on real 3D scene data.

Overall, our contributions are three-fold: 1) We ex-hume Human-Occupancy Interaction as a major component of static HSI. 2) By digging out the inherent Human-Occupancy relationships of pure motions, we convert the motion-only data into a paired Human-Occupancy database MOB, expanding the data scale. 3) We develop a versatile controller for interaction motion generation, which is flexible and stable.

## 2. Related Works

**Human-Scene Interaction Generation.** Generating natural human motion sequences has received increasing attention with the emerging MoCap datasets [6, 13, 22, 27, 30, 36]. Early efforts were paid to prefix/suffix-conditioned motion generation [2, 14, 15, 20], known as motion prediction and interpolation. There also have been efforts to pursue generating motion with respect to specific action semantics, either represented in action categories [12, 33, 53] or natural language [8, 13, 29, 34, 35, 47, 48, 57–59]. Audio-conditioned motion generation was also explored, like music for dance generation [25, 26]. However, these approaches tend to focus on human motion only, without placing the generated motion in a grounded 3D environment.

Recently, progress has been made to advance HSI generation. Kim *et al.* [23] first posed static human skeletons upon specific objects. Some [18, 60, 64] proceeded by placing SMPL-X [32] meshes in scanned 3D scenes. Semantic controls were also introduced [65]. For HSI motion genera-

tion, some [17, 40, 62] focused on interacting with a single target object, mostly chairs. GOAL [44] and SAGA [52] generated full-body pre-grasp motions. There have also been efforts [19, 46] for the physical control of specific interactions. With paired motion-scene datasets [1, 16], approaches that synthesize HSI motion in cluttered scenes appeared. Two-stage based algorithms [49, 50] were proposed to first generate static key-frame poses, and then interpolate them for a coherent motion. GAMMA [63] proposed an RL framework for locomotion on flat grounds with the help of off-the-shelf path-finding algorithms. DIMOS [66] extended GAMMA with extra interaction policies. In contrast, the follow-ups [1, 21, 51, 67] adopted a simple end-to-end one-stage paradigm, while focusing more on boosting data. GIMO [67] collected data with gaze information. HUMANISE [51] synthesized pseudo-data from large-scale motion bases and 3D scan bases. CIRCLE [1] collected data with a VR application. LAMA [24] coupled the RL framework with a motion-matching algorithm, generated HSI motions with only a unified policy, and leveraged motion editing for optimization. A major difference in our approach from previous efforts is our view of Human-Occupancy Interaction, which helps us to alleviate the data hunger, and also enables a unified controller. Moreover, we are the first to generate motion in a dynamic scene, which previous efforts failed to handle.

**Scene Creation from Motion.** There have also been efforts to synthesize plausible 3D scenes from human motion. Pose2Room [31] predicted 3D object bounding boxes from human motion. MOVER [55] reconstructed 3D scenes from videos that record human-scene interaction. SUMMON [54] and MIME [56] placed 3D object models with respect to human motion. These methods could be adopted to boost Human-Scene Interaction data. However, they are usually limited to a small range of indoor furniture.

### 3. Motion Occupancy Base

Human-scene interaction generation could be formulated as  $M = \mathcal{G}(S)$ , where  $M$  is the generated motion sequence,  $\mathcal{G}$  is the motion generator, and  $S$  is a 3D scene. Conventionally, the scene is expected to be as realistic as possible, requiring expensive acquisition. We find that these scenes could function almost equally to their occupancy for static HSI. Thus, high-quality scenes might become less necessary here. In view of this, we revisit the large-scale motion-only datasets. Intuitively, motion only contains body movement information. But if we switch our sight to the vacant space around the moving person, considering the space as *another form of occupancy*, we could find that these motions actually possess information on how humans interact with certain space occupancies. To this end, we aggregate motion-only datasets into the human-occupancy interaction database: Motion Occupancy Base (MOB).

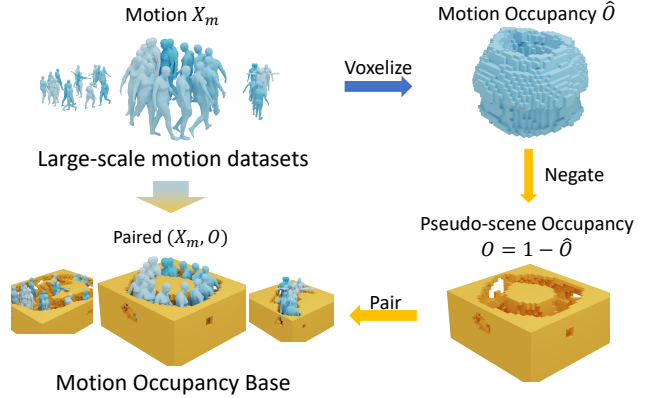


Figure 2. The construction process of Motion Occupancy Base.

The overall pipeline is shown in Fig. 2. Since we aim at the occupancy, motion data with SMPL(-X) [28, 32] representation is preferred. All the collected motions are re-sampled to 30 FPS and rotated so that the gravity direction points negative z-axis. For motion sequence  $X = \{x^i\}_{i=1}^t$ , where  $x_i$  is the SMPL(-X) representation in the  $i$ -th frame,  $t$  is the number of frames, we first obtain mesh sequence  $X_m = \{x_m^i\}_{i=1}^t$  via SMPL(-X) model, where  $x_m^i = (f^i, v^i)$  is the mesh for the  $i$ -th frame,  $f^i, v^i$  are the mesh faces and surface vertices. A bounding box of  $X_m$  is obtained based on vertices  $V = \{v_i\}_{i=1}^t$ . Given the predefined grid unit size  $u$ , the box region is voxelized into motion occupancy volume  $\hat{O} \in \{0, 1\}^{\{H \times W \times D\}}$ , whose content is computed in two steps: 1)  $V$  occupy the corresponding voxels in  $\hat{O}$ . 2) Given the centers of the unoccupied voxels as  $C = \{c_i\}_{i=1}^{|C|}$ , if  $c_i$  is inside any human mesh  $x_m^i$ , the corresponding voxel is occupied. The pseudo-scene occupancy  $O$  is then obtained by negating the motion occupancy, formulated as  $O = 1 - \hat{O}$ . Thus, for each motion-only sample  $X$ , we convert it into a motion-occupancy pair  $(X, O)$  in MOB. Finally, MOB aggregates 13 datasets, resulting in 98k instances. More statistics are in the supplementary materials.

As shown in Fig. 2, humans in MOB are acting with rather strict geometric constraints, which is uncommon in regular scenes covered by existing datasets [1, 16, 51]. However, we show that by learning from hard cases in MOB, our model could grow its ability to handle both complex and regular scenarios well.

## 4. Versatile Motion Controller

### 4.1. Preliminaries

Recall the  $M = \mathcal{G}(S)$  formulation for HSI generation. Previous efforts either directly adopt a one-shot transformer generator, or decompose  $\mathcal{G}$  into two separate generators, one for interaction key-frame generation, the other for key-

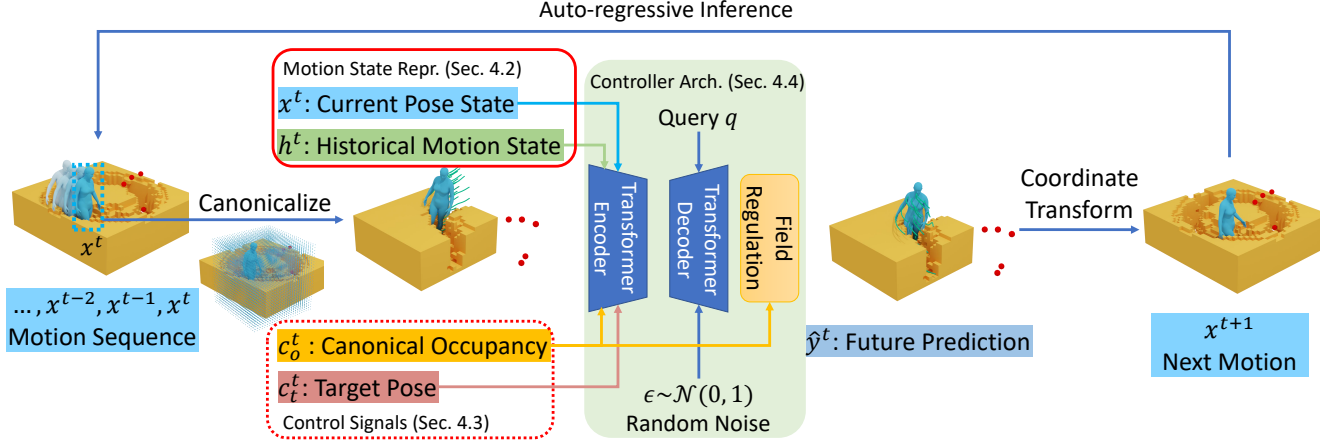


Figure 3. The architecture of our versatile motion controller. Given motion state and histories  $x^t, h^t$ , and control signals  $c_o^t, c_t^t$ , the controller auto-regressively generates the next motion frame w.r.t. the target pose and the canonical occupancy.

frame interpolation. Differently, we formulate our generator as an auto-regressive motion controller. At time step  $t$ , given historical motion state  $h^t$ , current pose state  $x^t$ , we aim at learning such a controller as

$$\hat{y}^t = \mathbf{G}(h^t, x^t, c^t), \quad (1)$$

where  $\hat{y}^t$  is the predicted future motion, and  $c^t$  is the control signals including target pose and canonical space occupancy. An overview is illustrated in Fig. 3. Sec. 4.2 introduces motion state representation  $h^t, x^t, y^t$ . The control signals are covered in Sec. 4.3. Then, the controller architecture is detailed in Sec. 4.4. Finally, Sec. 4.5 demonstrates the training and inference procedure of the controller.

## 4.2. Motion State Representation

**Notations.** In the global coordinate, we represent motion sequence  $X$  with  $T$  frames as  $X = \{x^t\}_{t=1}^T$ , where  $x^t = (p_r^t, \theta_r^t, r^t)$  is SMPL [28] parameters, with root location  $p_r^t \in \mathcal{R}^3$ , root orientation  $\theta_r^t \in \mathcal{R}^6$ , and the orientation of  $j$  limbs as  $\theta^t \in \mathcal{R}^{j \times 6}$ . Based on this, the location of  $j$  joints  $p^t \in \mathcal{R}^{j \times 3}$  could also be computed via SMPL. For simplicity, we use  $\cdot^{-w}$  to represent the value from frame  $t-w$  to  $t$ , and  $\cdot^{+w}$  for  $t$  to  $t+w$ . The 6D form from [68] is adopted for all rotation and orientation representations.

**Current Pose State** could be formulated as

$$x^t = \text{Cano}(\{p_r^t, p^t, \theta_r^t, \theta^t, \dot{p}_r^t, \dot{p}^t, \dot{\theta}_r^t\}, t), \quad (2)$$

where  $\cdot^t$  indicates the first derivative of corresponding values at  $t$ .  $\text{Cano}(\cdot, t)$  canonicalizes the input with respect to the root location and facing direction at frame  $t$ , ensuring a consistent representation across different frames.

**Historical Motion State**  $h^t$  provides a contextual backdrop of the preceding motion dynamics from frame  $t-w$  to  $t$ , where  $w$  is the window size.  $h^t$  is formulated as

$$h^t = \text{Cano}(\{p_r^{-w}, p^{-w}, \theta_r^{-w}, \dot{p}_r^{-w}, \dot{p}^{-w}, \dot{\theta}_r^{-w}\}, t), \quad (3)$$

which contains trajectories  $p_r^{-w}, p^{-w}$ , root orientation  $\theta_r^{-w}$ , velocities  $\dot{p}_r^{-w}, \dot{p}^{-w}$ , and root angular velocity  $\dot{\theta}_r^{-w}$ . For conciseness, if not specified, only the  $p^{-w}$  of the hands and feet is adopted in practice,

**Future Prediction**  $\hat{y}^t$  is composed of two parts as

$$\hat{y}^t = \{\hat{x}^{t+1}, \hat{u}^t\}. \quad (4)$$

Note that  $\hat{x}^{t+1}$  is in the egocentric canonical of frame  $t$ , and  $\hat{p}_r, \hat{\theta} \subset \hat{x}^{t+1}$  are adopted to transit from  $t$  to  $t+1$ . Mirroring the historical motion state  $h^t$ , we also incorporate a comprehensive set of future trajectories, facing directions and their changing rates as  $\hat{u}^t = \{p_r^{+f}, p^{+f}, \theta^{+f}, \dot{p}_r^{+f}, \dot{p}^{+f}, \dot{\theta}^{+f}\}$  for a window size of  $f$ , all in the canonical view of  $t+1$ . Empirically, integrating  $\hat{u}^t$  significantly enhances the model’s precision in navigating toward the target.

## 4.3. Control Signals

In this section, we introduce how the different control signals are encoded. Note that these control signals are optional, and our models can operate without these signals.

**Canonical Occupancy.** A simple voxel-based representation is adopted to encode how the canonical space is occupied by the scenes. We utilize a cubic point grid  $o^t \in \{0, 1\}^{s \times s \times s}$  characterized by the grid size  $s$  and the grid unit size  $u$  at frame  $t$ . The grid is positioned in the human’s canonical space, with its center offset by  $s/4$  in the human-facing direction. Each cell contains a binary value, indicating whether the cell is intersecting with the global scene occupancy  $O$ . The canonical occupancy is thus represented as  $c_o^t = \text{Flatten}(o^t) \in \{0, 1\}^{s^3}$ .

**Target Pose** is also considered as a control signal. We characterize the target pose based on the positions of the root, hands, and feet, each defined in relation to the canonical space of the current pose, represented as  $c_t^t \in \mathcal{R}^{5 \times 3}$ .

In practice, these could be assigned manually or generated from off-the-shelf models [65]. Also, partial or blank targets are acceptable.

#### 4.4. Controller Architecture

We adopt a lightweight transformer-based architecture. We first adopt  $n$  fully connected layers to project the  $n$  input features from  $\{h^t, x^t, c^t\}$  to the latent space of our model as latent  $z \in \mathcal{R}^{n \times d}$ . The latent feature  $z$  is then fed into encoder  $E$  to distill dynamic information from the motion states and control signals. To enhance information interchange and to produce a more refined embedding, we devise  $E$  as a sequence of Transformer encoders, which takes  $z$  as input and outputs refined dynamic information  $\hat{z} = E(z) \in \mathcal{R}^{n \times d}$ . Finally, we adopt a transformer decoder  $D$  followed by a linear layer to condense the dynamic information, resulting in the final predictions. With learnable query  $q \in \mathcal{R}^d$  and the dynamic information  $\hat{z}$  serving as K and V, respectively, the output of the transformer is further concatenated with a random noise  $\epsilon \in \mathcal{R}^d$  for randomness. The linear layer then outputs the final prediction as  $\hat{y}^t = D(\hat{z}, q, \epsilon)$ .

Furthermore, we introduce a novel module called **Field Regulation** to enhance collision avoidance. The basic idea is that humans tend to move faster in obstacle-sparse areas and decelerate in complex environments or when an obstacle is nearby. At very short distances, especially when an imminent collision would happen, a complete halt is necessary. Given this, we propose *Occupancy Field*, which exerts negligible influence on humans at a distance but escalates to a sturdy repulsion as proximity increases, thereby compelling the human to decelerate and ultimately come to a standstill. The occupancy field influences human motion only when a human is in motion toward it. The field functions as

$$\Delta \dot{p}_j^{t+1} = \mathcal{F}(\dot{p}_j^{t+1}, c_o^t). \quad (5)$$

The field  $\mathcal{F}$  calculates a correction  $\Delta \dot{p}^{t+1}$  based on predicted joint velocity  $\dot{p}_j^{t+1} \in \{\dot{p}_r^{t+1}, \dot{p}^{t+1}\}$  and canonical occupancy  $c_o^t$ , which is then added to the velocity  $\dot{p}^{t+1}$ . For simplicity, the superscripts indicating the time steps are omitted in the following equations. In detail, given the center points of all the occupied voxels in  $c_o$  as  $P \subset \mathcal{R}^{n_p \times 3}$ , the correction is calculated as

$$\Delta \dot{p}_j = \sum_{P_i \in P} -k r_i \max \left( 0, \frac{1}{\|v_{ij}\|_a - \gamma} - b \right), \quad (6)$$

$$r_i = \dot{p}_j \max(0, \langle \dot{p}_j, v_{ij} \rangle), \quad (7)$$

where  $v_{ij} = P_i - p_j$  is the vector from the joint  $j$  to the voxel center,  $\langle \cdot, \cdot \rangle$  indicates the cosine between the two vectors,  $\|\cdot\|_a$  denotes  $a$ -norm, and  $k$  is the stiffness factor.  $\gamma$  and  $b$  are thresholds to constrain the distance range of effective voxels, where  $\gamma$  reflects the human body's width and voxels

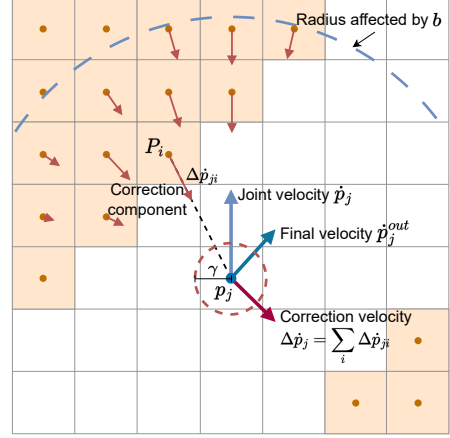


Figure 4. Field Regulation. Occupied voxel centers  $\{P_i\}$  are located at the top left of the figure. The initial velocity vector,  $\dot{p}_j$ , is directed upwards, posing a risk of collision. To mitigate this, the occupancy field introduces a corrective velocity component  $\Delta \dot{p}_j$ . This redirects the final velocity  $\dot{p}_j^{out}$  to avoid collision.

within this range are discounted for stability. An illustration of Field Regulation is shown in Fig. 4. The field regulation is incorporated in the controller's training to adapt to it, avoiding potential foot sliding caused due to direct modification on velocities. Extensive experiments show that Field Regulation is considerably effective in reducing collision.

#### 4.5. Training and Inference

**Training Objectives** The controller is trained in a fully-supervised manner. We employ a mixture of L1 and L2 losses as basic objectives. Besides, penetration loss and occupancy field loss are designed to hinder undesired collisions. Specifically, L1 loss is utilized for rotation-related output values  $\hat{y}_\theta^t \in \hat{y}^t$ , while L2 loss is applied to the rest outputs  $\hat{y}_p^t$ . The mixture loss could be formulated as

$$\mathcal{L}_{mix} = \|\hat{y}_\theta^t - \hat{y}_\theta^t\|_1 + \|\hat{y}_p^t - \hat{y}_p^t\|_2. \quad (8)$$

Given the predicted joint location  $\hat{p}^{t+1}$ , penetration loss is computed as

$$\mathcal{L}_{pen} = \sum_{i=0}^j O(\hat{p}_j^{t+1}) \|ref(\hat{p}_j^{t+1}, O)\|_2, \quad (9)$$

where  $O(\cdot)$  returns 1 if the point is occupied in  $O$  else 0, and  $ref(\hat{p}_j^{t+1}, O)$  calculates the closest unoccupied voxel center in  $O$  for joint  $\hat{p}_j^{t+1}$ . Occupancy field loss has two components. First, to deter undesired interactions, we penalize the proportion of the occupancy field effect relative to the output root velocity. Second, observing occasional unnatural spikes in velocity, where the human figure seemingly attempts to navigate through an obstacle, we punish excessive velocities. The occupancy field loss is formulated

Method	Suc. (%) $\uparrow$	DT (cm) $\downarrow$	Time (s)	FS (%)	PEN $\downarrow$	ERP
GT	100.00	0.00	3.00	3.36	0.00	-
DIMOS [66]	15.73	48.97	6.82	10.52	123.12	6.82
w/o Occ.	71.22	<b>14.66</b>	<b>2.25</b>	<b>6.89</b>	46.05	4.13
Ours	<b>77.91</b>	15.30	3.62	8.13	<b>15.21</b>	4.24

Table 1. Quantitative results on MOB.

as

$$\mathcal{L}_{field} = \left( \frac{|\Delta \dot{p}|}{|\dot{p}|} \right)^2 + |\dot{p}|^2. \quad (10)$$

The final loss is computed as

$$\mathcal{L} = \mathcal{L}_{mix} + \alpha \mathcal{L}_{pen} + \beta \mathcal{L}_{field}, \quad (11)$$

where  $\alpha$  and  $\beta$  are coefficients to balance the loss terms.

**Auto-regressive Inference** In our method, motion generation is performed in an auto-regressive manner, enabling the model to adapt to dynamic environmental changes. While the model solely manipulates canonical information, we track the global root position  $p_g$  and the facing direction  $\theta_g$  of the human in the world coordinate system. Initially, we set all input past and current velocities  $\dot{p}^0$  to zero. Before each prediction at frame  $t$ , we compute the control signals (if there are any), *i.e.*, the relative target position  $c_t^t$  and the canonical space occupancy  $c_o^t$ , based on the current values of  $p_g^t$  and  $\theta_g^t$ . After the prediction, we update  $p_g^t$  and  $\theta_g^t$  with the model’s output, along with the current pose state  $c^{t+1}$ . Concurrently, we refresh the historical motion state  $h^{t+1}$  to prepare for the next input.

## 5. Experiments

In this section, we show that our proposed controller could be applied to various HSI scenarios once trained on MOB.

**Implementation Details.** The controller consists of a two-layer transformer encoder and a single-layer transformer decoder, both with a latent dimension of 512 and 8 heads. The canonical occupancy grid size is set as (25, 25, 25), with a unit size of 8 cm. The controller operates at 10 FPS with the history and future window sizes both set as 1, which empirically brings more stable outcomes. The controller is trained on the MOB, with 1,393 sequences excluded from training as the test set. We train the controller for 75k iterations, with a cosine learning rate decay restart strategy. The initial learning rate is set as 1e-4. The control signals are randomly masked for augmentation during training. Scheduled Sampling [3] is adopted to increase stability. The whole training takes approximately 6 hours on a single 12G NVIDIA Titan Xp. For more details, please refer to the supplementary materials.

### 5.1. Interacting with Occupancy from MOB

We first evaluate the ability to interact with occupancy volumes with a goal-reaching task on MOB. Given an occupancy volume, a starting pose, and a target end-effector

pose, the model is required to generate transition motion from the starting pose to the target pose. We split the test set into 30k 3-second clips, adopting the first frame as the starting pose and the final frame as the target pose. The models are required to generate motion for 10s towards the target. There are two reasons for this setting. First, we would like to provide enough time for the models to accomplish the tasks. Second, we are also curious about how the models would behave after the target is reached and no new target is given, or when a very close target is given. The results are evaluated from three aspects.

**Task Completion** is determined by whether the target pose is reached. The target is identified as completed if the average Euclidean distance between the generated pose and the target pose is lower than 20 centimeters and less than 50 voxels are penetrated. We report the success rate (Suc.). The average minimum distance to the target pose (DT) and the time taken to accomplish the target are also reported for reference. Note that the time taken to accomplish the task is only calculated upon successful samples.

**Motion Quality** is evaluated via foot sliding (FS) and penetration (PEN) detection. A frame is identified as FS with its foot velocity  $>7.5$  cm/s following GAMMA [63]. We report the percentage of frames with FS. For PEN, we report the number of voxels penetrated per frame.

**Similarity to Dataset** is measured by the similarity between the predicted and GT target end-effector trajectory. We report Edit distance for the real penalty (ERP) [7] since the trajectories might have different lengths. It is only given as a reference, which is not the lower the better.

**Quantitative results** are shown in Tab. 1. For DIMOS [66], we convert the target pose into corresponding marker sets and report the best results from different policies for each test sample. For w/o Occ., we simply remove the canonical occupancy-related components. DIMOS frequently fails to get close to the goal successfully in complex scenarios, which we will elucidate later with qualitative results. Our models outperform DIMOS by a considerable margin with a single controller compared to multiple policies. This reveals that the straightforward voxel-based representation is capable of encoding holistic information for human-occupancy interaction. The model without occupancy manages to approach the target as closely and quickly as possible. However, it suffers from more severe interpenetration with the occupancy, resulting in a lower success rate. Instead, our model with consideration of occupancy behaves more conservatively, spending more time to accomplish the tasks with less penetration. A slightly higher foot sliding rate is also observed, which is a trade-off for the penetration-avoiding ability that field regulation brings.

**Qualitative results** are shown in Fig. 5, 6. Given the complex occupancy, previous state-of-the-art DIMOS [66] frequently fails to reach the goal due to the path-finding

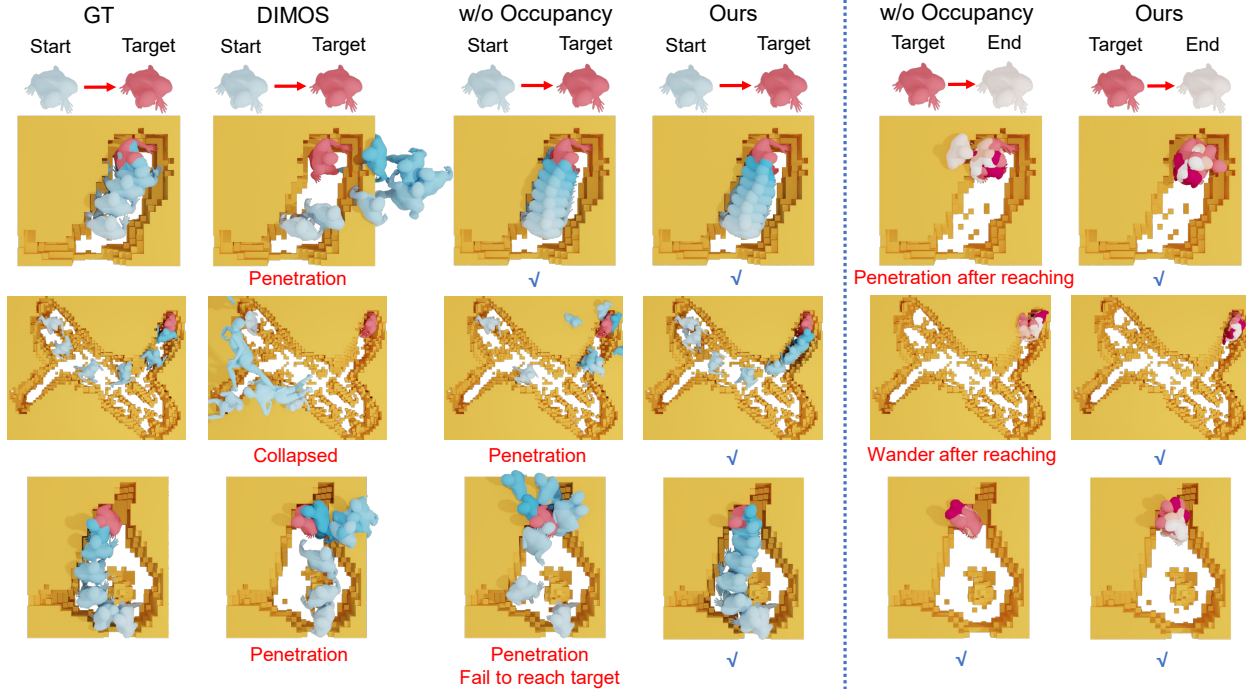


Figure 5. Our controller generates natural motions (white to blue) reaching the target (red) given the complex occupancy. Furthermore, the controller is capable of stabilizing the motions (red to white) around the targets after reaching them. Previous SOTA [66] suffers from severe penetration and fails to reach the target.

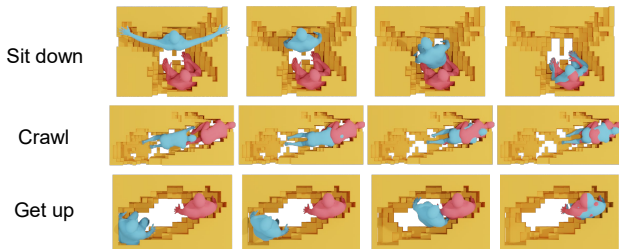


Figure 6. With the unified view of human-occupancy interaction, the same controller in Fig. 5 could conduct diverse motions.

algorithm adopted tends to fail in complex scenarios with corrupted sequences. This explains the unsatisfying quantitative results of DIMOS. Even when it reaches the goal, severe penetration is usually observed. Instead, our controller generates feasible motions to reach the targets. The typical locomotion-interaction decomposition [50, 63, 66] of previous methods tends to over-simplify both, with locomotion only focusing on foot walkability and interaction restricted to limited categories. It might be okay for spacious rooms, however, when posed in a cramped scene or scene with complex geometric structures like in Fig. 5, models could fail to find the path to the target and degenerate. In contrast, with our unified view of Human-Occupancy interaction, our controller applies to various scenarios beyond simplified locomotion and interaction. Furthermore, diverse

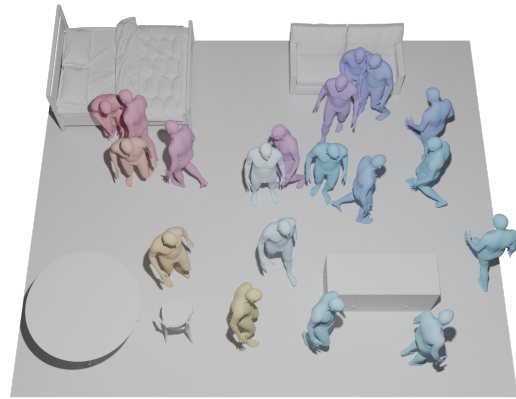


Figure 7. Our controller successfully adapts to the synthesized test room and is able to generate long-term motions. In this figure, a human circumnavigates a cabinet (cyan), sits on a sofa (blue), perches on a bed (magenta), and then resumes walking (yellow).

motions could be performed by the same controller (Fig. 6). By comparing our controllers with and without occupancy, we find that training with occupancy helps to avoid penetration significantly. Also, the controller with occupancy could stabilize the motion around the target after reaching it, while its counterpart tends to wander further inertially.

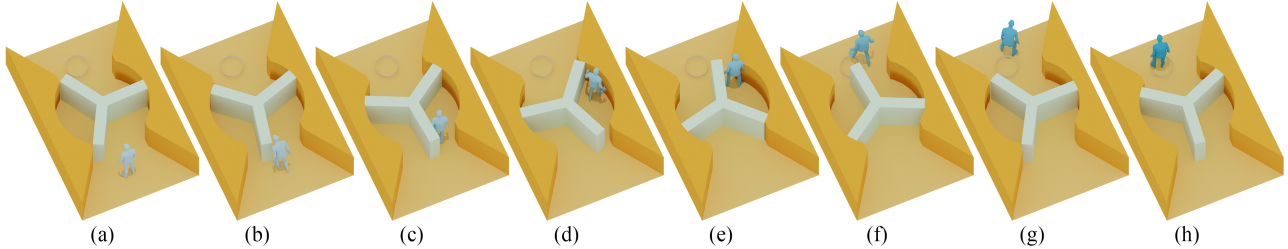


Figure 8. Our model is capable of avoiding dynamic obstacles and performing reasonable motion towards targets (circle).

Method	Suc. (%) $\uparrow$	DT (cm) $\downarrow$	Time (s)	FS (%)	PEN $\downarrow$	ERP
Ours	<b>77.91</b>	15.30	3.62	8.13	<b>15.21</b>	4.24
Ours w/o $L_{pen}$	74.14	14.89	3.54	7.89	31.93	4.96
Ours w/o $L_{field}$	75.34	15.69	2.86	11.65	25.83	5.70
Ours w/o FR	77.38	<b>14.85</b>	<b>2.34</b>	<b>6.57</b>	33.49	4.18
Ours w/ BPS	73.64	16.83	3.35	9.34	36.72	4.72

Table 2. Ablative results on MOB.

## 5.2. Interacting with Static Scenes

Once our controller is trained on the more complex MOB, it could be effortlessly applied to realistic synthesized rooms and scene scans. We test our model in a synthetic test room from DIMOS [66] in Fig. 7 and a realistic scan from Replica [41] in Fig. 1. The occupancy is transferred from the scene SDFs. In both environments, our model produces convincing motions, navigates around obstacles, and transitions seamlessly between locomotion and interaction. Remarkably, it adapts to sitting on various objects, such as sofas, a bed, and a stool, revealing its versatility in recognizing different occupancies with appropriate height as potential seats. The test room features sparse furnishings, highlighting the model’s ability to operate in open spaces diverging from MOB samples. Conversely, the Replica scene presents a more cluttered setup. Here, the model adeptly maneuvers through tight spaces, avoids overlapping with objects, and produces plausible movements. Furthermore, our model is able to generate long-term motions. The motions in Fig. 1 and Fig. 7 are generated in a single attempt by merely altering the target, both spanning around 30 seconds, which are clipped from longer motions for clear illustration in the limited space. More results are in the supplementary materials.

## 5.3. Interacting with Dynamic Scenes

We demonstrate the interaction in dynamic environments with a custom automatic door scenario in Fig. 8. With the target (the circle) in front of the human (a), it initially attempts to walk forward (b). However, this is blocked by the door, prompting our model to divert to the right (c). As the human walks faster than the door rotates, it confronts a temporary blockage caused by the conjunction of the wall and the door (d). Rather than breaching the barrier, the human adapts its speed with the door and sidesteps (e). Upon the

door granting sufficient clearance, the human resumes its course toward the target (f). After a slight overshoot past the target (g), it steps backward and halts precisely at the target location (h). This sequence exemplifies the model’s ability to adapt to and navigate within a dynamic environment, displaying realistic and contextually appropriate motion. More details are available in the supplementary materials.

## 5.4. Ablation Studies

With our controller as the baseline, selected ablation studies on MOB are reported in Tab. 2. Complete results and details are included in the supplementary.

**Different loss terms.** By removing penetration loss  $L_{pen}$ , a major degeneration in Success rate and PEN is observed. This shows that explicitly punishing penetration is necessary. The removal of  $L_{field}$  also hurts the success rate by 2.57%, with PEN increasing by 10.62. FS also increases notably. We identify that without  $L_{field}$ , the field regulation would generate unnatural spikes.

**Field Regulation (FR)** is also evaluated. Eliminating the field regulation decreases the success rate slightly, with a notable PEN increase (+18.28) and FS decrease (-1.56%), revealing the tradeoff it conducts between PEN and FS.

**Occupancy representation.** We replaced the voxel-based representation of canonical occupancy with the more compact and efficient BPS [37]. The field regulation is also modified accordingly. Degradation is observed in most metrics. Despite its efficiency, BPS might ignore too much information and bring instability to the field regulation.

## 6. Conclusion

By identifying the major component of static HSI as Human-Occupancy Interaction, we revisited static HSI from a unified space occupancy view. Large-scale Human Occupancy Interaction database MOB was aggregated from motion-only data, which substantially improved diversity and complexity. Moreover, a versatile auto-regressive controller was trained on MOB for Human-Occupancy Interaction generation, which supports flexible and stable generation for static HSI under a spectrum of scenarios without training with real 3D scene data. Extending the controller for more forms of control signals like finer-

grained poses, language commands, and scene attributes would be an interesting future direction. Also, we are looking forward to exploring interactions that change the scene with this space-occupancy view in future work.

## References

- [1] Joao Pedro Araújo, Jiaman Li, Karthik Vetrivel, Rishi Agarwal, Jiajun Wu, Deepak Gopinath, Alexander William Clegg, and Karen Liu. Circle: Capture in rich contextual environments. In *Proceedings of the IEEE/CVF Conference on Computer Vision and Pattern Recognition*, pages 21211–21221, 2023. [2](#), [3](#), [1](#)
- [2] Nikos Athanasiou, Mathis Petrovich, Michael J Black, and Gül Varol. Teach: Temporal action composition for 3d humans. In *2022 International Conference on 3D Vision (3DV)*, pages 414–423. IEEE, 2022. [2](#)
- [3] Samy Bengio, Oriol Vinyals, Navdeep Jaitly, and Noam Shazeer. Scheduled sampling for sequence prediction with recurrent neural networks. *Advances in neural information processing systems*, 28, 2015. [6](#)
- [4] Bharat Lal Bhatnagar, Xianghui Xie, Ilya Petrov, Cristian Sminchisescu, Christian Theobalt, and Gerard Pons-Moll. Behave: Dataset and method for tracking human object interactions. In *IEEE Conference on Computer Vision and Pattern Recognition (CVPR)*. IEEE, 2022. [1](#)
- [5] Zhongang Cai, Mingyuan Zhang, Jiawei Ren, Chen Wei, Daxuan Ren, Zhengyu Lin, Haiyu Zhao, Lei Yang, and Ziwei Liu. Playing for 3d human recovery. *arXiv preprint arXiv:2110.07588*, 2021. [1](#)
- [6] Zhongang Cai, Daxuan Ren, Ailing Zeng, Zhengyu Lin, Tao Yu, Wenjia Wang, Xiangyu Fan, Yang Gao, Yifan Yu, Liang Pan, Fangzhou Hong, Mingyuan Zhang, Chen Change Loy, Lei Yang, and Ziwei Liu. Humman: Multi-modal 4d human dataset for versatile sensing and modeling. In *Computer Vision – ECCV 2022*, pages 557–577, Cham, 2022. Springer Nature Switzerland. [2](#)
- [7] Lei Chen and Raymond Ng. On the marriage of lp-norms and edit distance. In *Proceedings of the Thirtieth international conference on Very large data bases-Volume 30*, pages 792–803, 2004. [6](#)
- [8] Xin Chen, Biao Jiang, Wen Liu, Zilong Huang, Bin Fu, Tao Chen, and Gang Yu. Executing your commands via motion diffusion in latent space. In *Proceedings of the IEEE/CVF Conference on Computer Vision and Pattern Recognition*, pages 18000–18010, 2023. [2](#)
- [9] Zicong Fan, Omid Taheri, Dimitrios Tzionas, Muhammed Kocabas, Manuel Kaufmann, Michael J. Black, and Otmar Hilliges. ARCTIC: A dataset for dexterous bimanual hand-object manipulation. In *Proceedings IEEE Conference on Computer Vision and Pattern Recognition (CVPR)*, 2023. [1](#)
- [10] Mihai Fieraru, Mihai Zanfir, Elisabeta Oneata, Alin-Ionut Popa, Vlad Olaru, and Cristian Sminchisescu. Three-dimensional reconstruction of human interactions. In *The IEEE/CVF Conference on Computer Vision and Pattern Recognition (CVPR)*, 2020. [1](#)
- [11] Mihai Fieraru, Mihai Zanfir, Silviu-Cristian Pirlea, Vlad Olaru, and Cristian Sminchisescu. Aifit: Automatic 3d human-interpretable feedback models for fitness training. In *The IEEE/CVF Conference on Computer Vision and Pattern Recognition (CVPR)*, 2021. [1](#)
- [12] Chuan Guo, Xinxin Zuo, Sen Wang, Shihao Zou, Qingyao Sun, Annan Deng, Minglun Gong, and Li Cheng. Action2motion: Conditioned generation of 3d human motions. In *Proceedings of the 28th ACM International Conference on Multimedia*, pages 2021–2029, 2020. [2](#)
- [13] Chuan Guo, Shihao Zou, Xinxin Zuo, Sen Wang, Wei Ji, Xingyu Li, and Li Cheng. Generating diverse and natural 3d human motions from text. In *Proceedings of the IEEE/CVF Conference on Computer Vision and Pattern Recognition (CVPR)*, pages 5152–5161, 2022. [2](#), [1](#)
- [14] Wen Guo, Yuming Du, Xi Shen, Vincent Lepetit, Xavier Alameda-Pineda, and Francesc Moreno-Noguer. Back to mlp: A simple baseline for human motion prediction. In *Proceedings of the IEEE/CVF Winter Conference on Applications of Computer Vision*, pages 4809–4819, 2023. [2](#)
- [15] Félix G Harvey, Mike Yurick, Derek Nowrouzezahrai, and Christopher Pal. Robust motion in-betweening. *ACM Transactions on Graphics (TOG)*, 39(4):60–1, 2020. [2](#)
- [16] Mohamed Hassan, Vasileios Choutas, Dimitrios Tzionas, and Michael J. Black. Resolving 3D human pose ambiguities with 3D scene constraints. In *International Conference on Computer Vision*, pages 2282–2292, 2019. [2](#), [3](#), [1](#)
- [17] Mohamed Hassan, Duygu Ceylan, Ruben Villegas, Jun Saito, Jimei Yang, Yi Zhou, and Michael J Black. Stochastic scene-aware motion prediction. In *Proceedings of the IEEE/CVF International Conference on Computer Vision*, pages 11374–11384, 2021. [2](#), [3](#), [1](#)
- [18] Mohamed Hassan, Partha Ghosh, Joachim Tesch, Dimitrios Tzionas, and Michael J Black. Populating 3d scenes by learning human-scene interaction. In *Proceedings of the IEEE/CVF Conference on Computer Vision and Pattern Recognition*, pages 14708–14718, 2021. [2](#)
- [19] Mohamed Hassan, Yunrong Guo, Tingwu Wang, Michael Black, Sanja Fidler, and Xue Bin Peng. Synthesizing physical character-scene interactions. In *ACM SIGGRAPH 2023 Conference Proceedings*, New York, NY, USA, 2023. Association for Computing Machinery. [3](#)
- [20] Alejandro Hernandez, Jurgen Gall, and Francesc Moreno-Noguer. Human motion prediction via spatio-temporal inpainting. In *Proceedings of the IEEE/CVF International Conference on Computer Vision*, pages 7134–7143, 2019. [2](#)
- [21] Siyuan Huang, Zan Wang, Puhao Li, Baoxiong Jia, Tengyu Liu, Yixin Zhu, Wei Liang, and Song-Chun Zhu. Diffusion-based generation, optimization, and planning in 3d scenes. In *Proceedings of the IEEE/CVF Conference on Computer Vision and Pattern Recognition*, pages 16750–16761, 2023. [2](#), [3](#)
- [22] Yanli Ji, Feixiang Xu, Yang Yang, Fumin Shen, Heng Tao Shen, and Wei-Shi Zheng. A large-scale rgb-d database for arbitrary-view human action recognition. In *Proceedings of the 26th ACM international Conference on Multimedia*, pages 1510–1518, 2018. [2](#)

- [23] Vladimir G Kim, Siddhartha Chaudhuri, Leonidas Guibas, and Thomas Funkhouser. Shape2pose: Human-centric shape analysis. *ACM Transactions on Graphics (TOG)*, 33(4):1–12, 2014. [2](#)
- [24] Jiye Lee and Hanbyul Joo. Locomotion-action-manipulation: Synthesizing human-scene interactions in complex 3d environments. In *Proceedings of the IEEE/CVF International Conference on Computer Vision (ICCV)*, pages 9663–9674, 2023. [3](#)
- [25] Ruilong Li, Shan Yang, David A Ross, and Angjoo Kanazawa. Learn to dance with aist++: Music conditioned 3d dance generation. *arXiv preprint arXiv:2101.08779*, 2(3), 2021. [2](#), [1](#)
- [26] Ruilong Li, Shan Yang, David A Ross, and Angjoo Kanazawa. Ai choreographer: Music conditioned 3d dance generation with aist++. In *Proceedings of the IEEE/CVF International Conference on Computer Vision*, pages 13401–13412, 2021. [2](#)
- [27] Jing Lin, Ailing Zeng, Shunlin Lu, Yuanhao Cai, Ruimao Zhang, Haoqian Wang, and Lei Zhang. Motion-x: A large-scale 3d expressive whole-body human motion dataset. *arXiv preprint arXiv:2307.00818*, 2023. [2](#)
- [28] Matthew Loper, Naureen Mahmood, Javier Romero, Gerard Pons-Moll, and Michael J Black. Smpl: A skinned multi-person linear model. *ACM transactions on graphics (TOG)*, 34(6):1–16, 2015. [3](#), [4](#)
- [29] Thomas Lucas, Fabien Baradel, Philippe Weinzaepfel, and Grégory Rogez. Posegpt: quantization-based 3d human motion generation and forecasting. In *Computer Vision—ECCV 2022: 17th European Conference, Tel Aviv, Israel, October 23–27, 2022, Proceedings, Part VI*, pages 417–435. Springer, 2022. [2](#)
- [30] Naureen Mahmood, Nima Ghorbani, Nikolaus F Troje, Gerard Pons-Moll, and Michael J Black. Amass: Archive of motion capture as surface shapes. In *Proceedings of the IEEE/CVF international conference on computer vision*, pages 5442–5451, 2019. [2](#), [1](#)
- [31] Yinyu Nie, Angela Dai, Xiaoguang Han, and Matthias Nießner. Pose2room: understanding 3d scenes from human activities. In *European Conference on Computer Vision*, pages 425–443. Springer, 2022. [3](#)
- [32] Georgios Pavlakos, Vasileios Choutas, Nima Ghorbani, Timo Bolkart, Ahmed A. A. Osman, Dimitrios Tzionas, and Michael J. Black. Expressive body capture: 3D hands, face, and body from a single image. In *Proceedings IEEE Conf. on Computer Vision and Pattern Recognition (CVPR)*, pages 10975–10985, 2019. [2](#), [3](#)
- [33] Mathis Petrovich, Michael J Black, and Gül Varol. Action-conditioned 3d human motion synthesis with transformer vae. In *Proceedings of the IEEE/CVF International Conference on Computer Vision*, pages 10985–10995, 2021. [2](#)
- [34] Mathis Petrovich, Michael J Black, and Gül Varol. Temos: Generating diverse human motions from textual descriptions. In *Computer Vision—ECCV 2022: 17th European Conference, Tel Aviv, Israel, October 23–27, 2022, Proceedings, Part XXII*, pages 480–497. Springer, 2022. [2](#)
- [35] Mathis Petrovich, Michael J. Black, and Gül Varol. Tmr: Text-to-motion retrieval using contrastive 3d human motion synthesis. In *Proceedings of the IEEE/CVF International Conference on Computer Vision (ICCV)*, pages 9488–9497, 2023. [2](#)
- [36] Matthias Plappert, Christian Mandery, and Tamim Asfour. The kit motion-language dataset. *Big data*, 4(4):236–252, 2016. [2](#)
- [37] Sergey Prokudin, Christoph Lassner, and Javier Romero. Efficient learning on point clouds with basis point sets. In *Proceedings of the IEEE International Conference on Computer Vision*, pages 4332–4341, 2019. [8](#), [1](#)
- [38] Xavi Puig, Eric Undersander, Andrew Szot, Mikael Dallaire Cote, Ruslan Partsey, Jimmy Yang, Ruta Desai, Alexander William Clegg, Michal Hlavac, Tiffany Min, Theo Gervet, Vladimír Vondruš, Vincent-Pierre Berges, John Turner, Oleksandr Maksymets, Zsolt Kira, Mrinal Kalakrishnan, Jitendra Malik, Devendra Singh Chaplot, Unnat Jain, Dhruv Batra, Akshara Rai, and Roozbeh Mottaghi. Habitat 3.0: A co-habitat for humans, avatars and robots, 2023. [1](#)
- [39] Manolis Savva, Abhishek Kadian, Oleksandr Maksymets, Yili Zhao, Erik Wijmans, Bhavana Jain, Julian Straub, Jia Liu, Vladlen Koltun, Jitendra Malik, Devi Parikh, and Dhruv Batra. Habitat: A Platform for Embodied AI Research. In *Proceedings of the IEEE/CVF International Conference on Computer Vision (ICCV)*, 2019. [1](#)
- [40] Sebastian Starke, He Zhang, Taku Komura, and Jun Saito. Neural state machine for character-scene interactions. *ACM Trans. Graph.*, 38(6):209–1, 2019. [1](#), [3](#)
- [41] Julian Straub, Thomas Whelan, Lingni Ma, Yufan Chen, Erik Wijmans, Simon Green, Jakob J Engel, Raul Mur-Artal, Carl Ren, Shobhit Verma, et al. The replica dataset: A digital replica of indoor spaces. *arXiv preprint arXiv:1906.05797*, 2019. [8](#)
- [42] Andrew Szot, Alex Clegg, Eric Undersander, Erik Wijmans, Yili Zhao, John Turner, Noah Maestre, Mustafa Mukadam, Devendra Chaplot, Oleksandr Maksymets, Aaron Gokaslan, Vladimír Vondrus, Sameer Dharur, Franziska Meier, Wojciech Galuba, Angel Chang, Zsolt Kira, Vladlen Koltun, Jitendra Malik, Manolis Savva, and Dhruv Batra. Habitat 2.0: Training home assistants to rearrange their habitat. In *Advances in Neural Information Processing Systems (NeurIPS)*, 2021. [1](#)
- [43] Omid Taheri, Nima Ghorbani, Michael J. Black, and Dimitrios Tzionas. GRAB: A dataset of whole-body human grasping of objects. In *ECCV*, 2020. [1](#)
- [44] Omid Taheri, Vasileios Choutas, Michael J Black, and Dimitrios Tzionas. Goal: Generating 4d whole-body motion for hand-object grasping. In *Proceedings of the IEEE/CVF Conference on Computer Vision and Pattern Recognition*, pages 13263–13273, 2022. [3](#)
- [45] Yansong Tang, Jinpeng Liu, Aoyang Liu, Bin Yang, Wenxun Dai, Yongming Rao, Jiwen Lu, Jie Zhou, and Xiu Li. Flag3d: A 3d fitness activity dataset with language instruction. *arXiv preprint arXiv:2212.04638*, 2022. [1](#)
- [46] Chen Tessler, Yoni Kasten, Yunrong Guo, Shie Mannor, Gal Chechik, and Xue Bin Peng. Calm: Conditional adversarial latent models for directable virtual characters. In *ACM SIGGRAPH 2023 Conference Proceedings*, New York, NY, USA, 2023. Association for Computing Machinery. [3](#)

- [47] Guy Tevet, Brian Gordon, Amir Hertz, Amit H Bermano, and Daniel Cohen-Or. Motionclip: Exposing human motion generation to clip space. In *Computer Vision–ECCV 2022: 17th European Conference, Tel Aviv, Israel, October 23–27, 2022, Proceedings, Part XXII*, pages 358–374. Springer, 2022. 2
- [48] Guy Tevet, Sigal Raab, Brian Gordon, Yoni Shafir, Daniel Cohen-or, and Amit Haim Bermano. Human motion diffusion model. In *The Eleventh International Conference on Learning Representations*, 2022. 2
- [49] Jiashun Wang, Huazhe Xu, Jingwei Xu, Sifei Liu, and Xiaolong Wang. Synthesizing long-term 3d human motion and interaction in 3d scenes. In *Proceedings of the IEEE/CVF Conference on Computer Vision and Pattern Recognition*, pages 9401–9411, 2021. 2, 3
- [50] Jingbo Wang, Yu Rong, Jingyuan Liu, Sijie Yan, Dahua Lin, and Bo Dai. Towards diverse and natural scene-aware 3d human motion synthesis. In *Proceedings of the IEEE/CVF Conference on Computer Vision and Pattern Recognition*, pages 20460–20469, 2022. 2, 3, 7
- [51] Zan Wang, Yixin Chen, Tengyu Liu, Yixin Zhu, Wei Liang, and Siyuan Huang. Humanise: Language-conditioned human motion generation in 3d scenes. *Advances in Neural Information Processing Systems*, 35:14959–14971, 2022. 2, 3
- [52] Yan Wu, Jiahao Wang, Yan Zhang, Siwei Zhang, Otmar Hilliges, Fisher Yu, and Siyu Tang. Saga: Stochastic whole-body grasping with contact. In *European Conference on Computer Vision*, pages 257–274. Springer, 2022. 3
- [53] Liang Xu, Ziyang Song, Dongliang Wang, Jing Su, Zhicheng Fang, Chenjing Ding, Weihao Gan, Yichao Yan, Xin Jin, Xiaokang Yang, Wenjun Zeng, and Wei Wu. Actformer: A gan-based transformer towards general action-conditioned 3d human motion generation. In *Proceedings of the IEEE/CVF International Conference on Computer Vision (ICCV)*, pages 2228–2238, 2023. 2
- [54] Sifan Ye, Yixing Wang, Jiaman Li, Dennis Park, C Karen Liu, Huazhe Xu, and Jiajun Wu. Scene synthesis from human motion. In *SIGGRAPH Asia 2022 Conference Papers*, 2022. 3
- [55] Hongwei Yi, Chun-Hao P Huang, Dimitrios Tzionas, Muhammed Kocabas, Mohamed Hassan, Siyu Tang, Justus Thies, and Michael J Black. Human-aware object placement for visual environment reconstruction. In *Proceedings of the IEEE/CVF Conference on Computer Vision and Pattern Recognition*, pages 3959–3970, 2022. 3
- [56] Hongwei Yi, Chun-Hao P. Huang, Shashank Tripathi, Lea Hering, Justus Thies, and Michael J. Black. Mime: Human-aware 3d scene generation. In *Proceedings of the IEEE/CVF Conference on Computer Vision and Pattern Recognition (CVPR)*, pages 12965–12976, 2023. 3
- [57] Jianrong Zhang, Yangsong Zhang, Xiaodong Cun, Yong Zhang, Hongwei Zhao, Hongtao Lu, Xi Shen, and Ying Shan. Generating human motion from textual descriptions with discrete representations. In *Proceedings of the IEEE/CVF Conference on Computer Vision and Pattern Recognition (CVPR)*, pages 14730–14740, 2023. 2
- [58] Mingyuan Zhang, Zhongang Cai, Liang Pan, Fangzhou Hong, Xinying Guo, Lei Yang, and Ziwei Liu. Motiondiffuse: Text-driven human motion generation with diffusion model. *arXiv preprint arXiv:2208.15001*, 2022.
- [59] Mingyuan Zhang, Xinying Guo, Liang Pan, Zhongang Cai, Fangzhou Hong, Huirong Li, Lei Yang, and Ziwei Liu. Remodiffuse: Retrieval-augmented motion diffusion model. In *Proceedings of the IEEE/CVF International Conference on Computer Vision (ICCV)*, pages 364–373, 2023. 2
- [60] Siwei Zhang, Yan Zhang, Qianli Ma, Michael J Black, and Siyu Tang. Place: Proximity learning of articulation and contact in 3d environments. In *2020 International Conference on 3D Vision (3DV)*, pages 642–651. IEEE, 2020. 2
- [61] Siwei Zhang, Qianli Ma, Yan Zhang, Zhiyin Qian, Taein Kwon, Marc Pollefeys, Federica Bogo, and Siyu Tang. Ego-body: Human body shape and motion of interacting people from head-mounted devices. In *European Conference on Computer Vision*, pages 180–200. Springer, 2022. 1
- [62] Xiaohan Zhang, Bharat Lal Bhatnagar, Sebastian Starke, Vladimir Guzov, and Gerard Pons-Moll. Couch: Towards controllable human-chair interactions. In *European Conference on Computer Vision*, pages 518–535. Springer, 2022. 2, 3
- [63] Yan Zhang and Siyu Tang. The wanderings of odysseus in 3d scenes. In *Proceedings of the IEEE/CVF Conference on Computer Vision and Pattern Recognition*, pages 20481–20491, 2022. 2, 3, 6, 7
- [64] Yan Zhang, Mohamed Hassan, Heiko Neumann, Michael J Black, and Siyu Tang. Generating 3d people in scenes without people. In *Proceedings of the IEEE/CVF conference on computer vision and pattern recognition*, pages 6194–6204, 2020. 2
- [65] Kaifeng Zhao, Shaofei Wang, Yan Zhang, Thabo Beeler, and Siyu Tang. Compositional human-scene interaction synthesis with semantic control. In *European Conference on Computer Vision*, pages 311–327. Springer, 2022. 2, 5
- [66] Kaifeng Zhao, Yan Zhang, Shaofei Wang, Thabo Beeler, and Siyu Tang. Synthesizing diverse human motions in 3d indoor scenes. In *Proceedings of the IEEE/CVF International Conference on Computer Vision (ICCV)*, pages 14738–14749, 2023. 2, 3, 6, 7, 8
- [67] Yang Zheng, Yanchao Yang, Kaichun Mo, Jiaman Li, Tao Yu, Yebin Liu, C Karen Liu, and Leonidas J Guibas. Gimo: Gaze-informed human motion prediction in context. In *European Conference on Computer Vision*, pages 676–694. Springer, 2022. 2, 3
- [68] Yi Zhou, Connelly Barnes, Jingwan Lu, Jimei Yang, and Hao Li. On the continuity of rotation representations in neural networks. In *Proceedings of the IEEE/CVF Conference on Computer Vision and Pattern Recognition*, pages 5745–5753, 2019. 4

# Revisit Human-Scene Interaction via Space Occupancy

## Supplementary Material

### Overview

- Section 7 introduces detailed statistics of the proposed Motion Occupancy Base.
- Section 8 introduces more details on the proposed versatile motion controller.
- Section 9 introduces details on the experiments.

### 7. Motion Occupancy Base Details

Dataset	#Motion
GTAHuman [5]*	40k
AMASS [30]	17.9k
FLAG3D [45]*	14.4k
CIRCLE [1]*†	14k
Fit3D [11]*	4.2k
GRAB [43]*†	2.7k
AIST++ [25]*	1.4k
ARCTIC [9]*†	1.2k
CHI3D [10]*	0.7k
BEHAVE [4]*†	0.6k
EgoBody [61]*	0.5k
SAMP [17]*†	0.3k
PROXD [16]*†	0.1k
Sum	98k

Table 3. Motion Occupancy Base statistics. \* means mirror augmentation is adopted for data boosting. † means the original dataset contains either scene or object information, but we do not use them.

MOB aggregates 13 datasets, resulting in 98k instances as shown in Tab. 3. Note that for all the datasets, we only preserve the motion data.

### 8. Versatile Motion Controller Details

In this section, we describe how we define the canonical space of a human. The coordinate system adopted in our work adheres to the right-hand rule. Following [13], we establish the human’s “right direction” by calculating the vector sum that extends from the left shoulder to the right shoulder and from the left hip to the right hip. Subsequently, the “forward direction” of the human is determined as the perpendicular vector to this “right direction” counterclockwise within the XY-plane. This approach facilitates an accurate and consistent orientation mapping for the human.

### 9. Experiment Details

#### 9.1. Implementation Details

The controller consists of a two-layer transformer encoder and a single-layer transformer decoder, both with a latent dimension of 512 and 8 heads. The canonical occupancy grid size is set as (25, 25, 25), with a unit size of 8 cm. For the BPS-based representation, the size is set as 1,024. The window sizes for the history and the future are both set as 1, which empirically brings more stable outcomes. The binary foot contact labels are included in the current pose, indicating whether the human’s feet are less than 5 cm to the ground, which slightly reduces foot skating. The controller operates at 10 FPS with the history and future window sizes both set as 1, which empirically brings more stable outcomes. The controller is trained on the MOB, with 1,393 sequences excluded from training as the test set. The training process spans 75k iterations, employing a cosine learning rate decay restart strategy, starting from an initial rate of  $1e-4$ . The loss coefficients are set as  $\alpha = 2, \beta = 1$ . For the Scheduled Sampling training strategy, we replace a subset of the inputs with the model’s outputs from the preceding timestamp, with the replacement probability  $p$  gradually increasing from 0 to 0.8 over the first 30 epochs. This procedure necessitates multi-step predictions at each training iteration, with our empirical choice being 4 steps. The whole training takes approximately 6 hours on a single 12G NVIDIA Titan Xp.

#### 9.2. Interaction with Dynamic Scenes

The scene features a circular, automatic revolving door with a radius of 1.5 m, providing space for entry and exit. This door assembly comprises three individual doors, each with a thickness of 35 cm. The doors are engineered to rotate around the Z-axis at a consistent speed of 15 degrees per second.

#### 9.3. Ablation Studies

For BPS-based [37] representation, a basis point set with 1,024 points is randomly sampled in a ball centered at the pelvis with a radius of 1m. The occupancy field is also considered upon the 1,024 points.